Available online at www.sciencedirect.com

SciVerse ScienceDirect

PHOTONICS AND NANOSTRUCTURES Fundamentals and Applications

Photonics and Nanostructures – Fundamentals and Applications 11 (2013) 335–344

www.elsevier.com/locate/photonics

Radiative coupling of high-order plasmonic modes with far-field

S. D'Agostino [a,*], F. Della Sala [b,c], L.C. Andreani [a]

[a] Dipartimento di Fisica, Università di Pavia, via Bassi 6, I-27100 Pavia, Italy

[b] National Nanotechnology Laboratory (NNL), Istituto Nanoscienze-CNR, Via per Arnesano 16, I-73100 Lecce, Italy

[c] Center for Biomolecular Nanotechnologies @UNILE, Istituto Italiano di Tecnologia, Via Barsanti, I-73010 Arnesano, Italy

Received 30 March 2013; received in revised form 13 June 2013; accepted 14 June 2013

Available online 24 June 2013

Abstract

In the last few years, hybrid systems consisting of punctual sources and metallic nanostructures have been assembled and studied. Furthermore, the radiative coupling between the two counterparts has become a crucial aspect to be explored in nanophotonics and plasmonics. In this paper a numerical framework based on the Discrete Dipole Approximation is presented as a simple computational scheme to analyze the decay dynamics of an emitter when it is located in the near proximities of metallic nanoparticles. This approach allows to go beyond the analytically solved cases and to predict the optical response of more complex shaped nanoparticles. Here the excitation of dipole and higher-order modes is studied as a function of the applied radiation with a particular attention paid to the changes induced in the response by approaching the source to the metal. Numerical results, obtained for Ag spheroids and conically shaped nanoparticles, are explained by analyzing the charge density induced on the surface of the nanoparticles, this allowing to distinguish dark from radiative modes in a straightforward way.

Keywords: Plasmonics; Nanoantennas; Dipole decay rates

1. Introduction

Over the last years the development of nano-optic techniques has affirmed the importance of exploiting plasmonic nanoantennas, like metallic nanoparticles or nanotips, to strongly enhance the absorption and the emission of radiation by a punctual receiver or emitter [1–7]. As is well known, thanks to the excitation of collective oscillations of the free electrons plasma (named localized surface plasmon resonances) [2], metallic nanostructures are able to enhance in a significant way the photonic density of states in their surroundings and in this way to strongly perturb the perturb the excitation and decay dynamics of proximate emitters, i.e. fluorophores or QDs [8]. Similar to radiowave and microwave antennas, their purpose is to convert the energy of free propagating radiation to localized energy, and vice versa. Several experimental works have demonstrated that the internal dynamics of any source of radiation can be tuned if the photonic environment is resonant with its radiative transitions [1,9–11]. Anyway, despite these evidences, the problem of mutual interaction between an emitter and a plasmonic antenna still presents lacking points and a lot of questions in molecular plasmonics results open, especially for what concerns complex-shaped nanoparticles that cannot be solved analytically.

For what concerns theory, the study of electrodynamic coupling between molecules and plasmonic antennas can be treated in different ways, according to

* Corresponding author. Tel.: +39 3407923120.
E-mail address: stefania.dagostino@unipv.it (S. D'Agostino).

1569-4410/$ – see front matter
http://dx.doi.org/10.1016/j.photonics.2013.06.003

the approximation adopted to describe the counterparts. Even if several options can be identified in literature, usually the molecule is described as a classical oscillating dipole, and the metal nanoparticle as a macroscopic entity characterized by its own frequency-dependent dielectric function [3].

In the work here presented, the description of the metal–emitter system and of the perturbations induced by metal on the decay dynamics of the emitter is performed in the framework of classical electrodynamics, well useful for weak-coupling regimes of interaction [12]. A numerical framework based on the Discrete Dipole Approximation (DDA) is applied: it turns out to be a simple and useful scheme to investigate coupling problems involving geometries which do not lend themselves to an analytical treatment. The idea underlying the analysis consists in accurately describing the nanoparticle shape through DDA to get a faithful description of the optical response of the metallic component to the emitter location, like recently done in literature with similar approaches [13–23]. The reliability of such numerical approach, as well as its generality in calculating the total and nonradiative decay rates has been recently demonstrated [24–26]. Here we are interested in the radiative behavior of the antenna. The radiative power of a polarizable system can be derived by starting from the flux of the Poynting vector through a surface enclosing it. Thus, being the scattered electric field in the far-field (radiation) zone due to the several multipoles in which the bound charge can be expanded (electric dipole, magnetic dipole, electric quadrupole and so on), it will contain contributions from modes of several order [27]. For metal nanoparticles whose dimensions are small if compared to the applied radiation wavelength, the major contribution to re-radiation can be ascribed to the dipole mode. The excited system assumes a fluctuating electric dipole moment and this causes electromagnetic radiation to be produced. Dipole radiation is thus considered the most important channel for radiative decay. Here we will show the potentialities and the criticalities of this approximation. Higher-order modes are not always dark modes and can produce a significant contribution in the electromagnetic coupling of plasmons with far field radiation. The analysis here reported aims at shedding light on the physical nature of the resonances appearing in the nanoparticles spectra and on the contributions that higher-order modes with respect to the dipolar one, can assume in large or elongated nanoparticles for which retardation effects can be significant and a net dipole moment different from zero can appear. In particular, a radiative contribution from the quadrupole mode is recognized for large silver prolate spheroids. This possibility for high-order modes to behave like bright modes is then confirmed by presenting the optical response of conically shaped nanoparticles to a plane wave excitation.

Numerical results, obtained for the different analyzed scatterers, assess that the decay rates of a dipole can be significantly tailored by tuning either the size or the shape of a nanoparticle and this could result of interest for measures of time-resolved fluorescence spectroscopy [28,29] and scanning near-optical microscopy [30,31].

2. Methods

The analysis here presented has been done in the framework of the Discrete Dipole Approximation [32] which is an useful method to numerically solve Maxwell equations for particles or arbitrary shapes and compositions. Also named *Coupled Dipole Approximation*, such numerical method is based on the discretization of the target into an array of N polarizable dipolar elements organized on a cubic lattice. The polarization of each element is the result of the interaction with the local electromagnetic field produced by all other elements plus the external field. The used implementation is ADDA [33,34] which allows to perform parallel simulations by partitioning the target into slices along one direction and thus to strongly reduce the run time. For what concerns the prescription for the polarizability, LDR (lattice dispersion relation) being this good enough to obtain a satisfactory level of accuracy ($<10\%$) for high discretization levels [35]. Here, like in other recent works [24–26], the ADDA code has been modified in order to consider dipolar fields as incident radiation. This should resemble the well known situation in molecular plasmonics, in which a metallic structure is irradiated by a point-like source like a chromophore or a small fluorophore. If we assume a point-like dipole $\tilde{\mathbf{p}}_0$ located at $\mathbf{r}_0$ and oscillating with frequency ω emitting electromagnetic radiation near a metallic nanoparticle, this nanoparticle will reflect and/or scatter back the radiation by generating an electric field $\tilde{\mathbf{E}}_{\mathrm{scat}}$ due to the polarization of the N internal dipoles. The idea underlying the present analysis is thus to numerically describe this key quantity. By solving in a self-consistent way a system of $3N$ coupled complex equations, DDA allows to calculated the N polarizabilities $\tilde{\mathbf{p}}_i$ describing the polarization response of the target to a particular excitation, so that the surface charge density as well as scattered field experienced by the dipole [36] can be easily calculated.

For what concerns the induced charge inside metal, the knowledge of the polarization field can easily be applied to obtain the informations needed. By recurring to the well known relation between the polarization of a material and its bound charge density, the charge density at any point $\mathbf{r}_i$ can be extracted

$$\tilde{\rho_i}(\mathbf{r}_i, \lambda_{\mathrm{exc}}) = -\nabla \cdot \tilde{\mathbf{P}}_{\mathrm{i}}(\mathbf{r}_i, \lambda_{\mathrm{exc}}) \tag{1}$$

and the surface charge distributions identified.

Another crucial quantity to compute is the response field or scattered field due to the localized surface plasmons induced in the nanoparticles. In weak-coupling regimes [37–40], starting from this quantity is possible to quantify the normalized spontaneous decay rate [16]

$$\frac{\Gamma}{\Gamma_0} = 1 + \frac{6\pi\varepsilon_0\tilde{\varepsilon}_B q_0}{k^3|\tilde{\mathbf{p}}_0|^2}\,\mathrm{Im}[\tilde{\mathbf{p}}_0^* \cdot \tilde{\mathbf{E}}_{\mathrm{scat}}(\mathbf{r}_0)] \tag{2}$$

where q_0 is the intrinsic quantum yield of the dipole, $\tilde{\varepsilon}_B$ is the relative dielectric constant of the background medium and Γ_0 is the decay rate of a dipolar emitter with unitary quantum efficiency ($q_0 = 1$). Eq. (2) expresses the modification of the lifetime of a molecule, known as the Purcell effect [41].

The optical reciprocity theorem [42] states that if the nanophotonic system is dissipative, the total decay rate Γ corresponds to the sum of radiative decay and the quenching rate induced by the loss environment [5,6,9]. For this reason the relation between the capability of an antenna to emit electromagnetic waves and its ability to collect them must be considered from the same point of view.

According to semiclassical theory [43], the non-radiative decay rate derives from the (time-averaged) power absorbed by the nanoparticle P_{abs} thus, by discretizing the nanoparticle within DDA, the normalized nonradiative decay rate Γ_{NR} becomes

$$\frac{\Gamma_{\mathrm{NR}}}{\Gamma_0} = \frac{6\pi\varepsilon_0^2\tilde{\varepsilon}_B Im(\tilde{\varepsilon})}{|\tilde{\mathbf{p}}_0|^2 k^3}\left(\sum_{i=1}^{N}\left|\tilde{\mathbf{E}}_{\mathrm{local}}(\mathbf{r}_i)\right|^2 \cdot V_c\right) \tag{3}$$

where the summation is done on the N dipoles contributions, V_c is the volume of each cubic element and $\tilde{\mathbf{E}}_{\mathrm{local}}$ is the total internal electric field given by $\tilde{\mathbf{P}}_i/(V_c\chi_i)$ where χ_i is the susceptibility of the medium at the dipole location. This quantity can thus be put into relation with the most common absorption cross section C_{abs}. It can be shown that for the used implementation ADDA the relation is given by

$$\frac{\Gamma_{\mathrm{NR}}}{\Gamma_0} = \frac{3\varepsilon_0^2\tilde{\varepsilon}_B}{8\pi|\tilde{\mathbf{p}}_0|^2 k^4} C_{\mathrm{abs}} \tag{4}$$

where C_{abs} is the standard absorption cross section calculated by a DDA simulation in which the field generated by the emitting dipole $\tilde{\mathbf{p}}_0$ is used as incident radiation

$$C_{\mathrm{abs}} = 4\pi k\sum_{i=1}^{N} Im(\tilde{\mathbf{p}}_i(\mathbf{r}_i) \cdot \tilde{\mathbf{E}}_i^*(\mathbf{r}_i)) \tag{5}$$

and the coefficient is obtained by considering the extra factor $1/(4\pi)^2$, deriving from the Gauss system used in ADDA [33,34].

The radiative decay rate can be finally obtained by computing the power radiated electromagnetically and dividing it by the photon energy $\hbar\omega$. It can thus be computed by calculating the flux of the Poynting vector through a surface enclosing the entire system (emitter plus nanoparticle). Beyond this direct method which does not include any limitations or approximation, it is also possible to get this quantity from the difference between Γ and Γ_{NR} in Eqs. (2) and (3) (we will refer to this method as indirect one, Γ_R^*). Usually the indirect method is preferred to the direct one only for computational reasons: as for the scattering cross sections, which can be considered the corresponding quantity, to make an integral on the whole solid angle requires a large computational effort, especially to reach sufficient convergence. Anyway, according to classical radiation theory the power radiated by a system which is much smaller in size than the wavelength of the emitted light is determined by the electric dipole moment [44]. If the electric dipole moment of the entire system (dipole of the NP plus external emitting dipole) is enhanced, so will the radiated power, the enhancement being proportional to the dipole amplification factor [42,43]

$$\frac{\Gamma_R}{\Gamma_0} = \frac{\varepsilon_0\tilde{\varepsilon}_B}{|\tilde{\mathbf{p}}_0|^2}\left|\left(\sum_{i=1}^{N}\tilde{\mathbf{p}}_i(\mathbf{r}_i)\right) + \tilde{\mathbf{p}}_0\right|^2. \tag{6}$$

While (2) and (3) give always an exact expression of the total and nonradiative decay rate, in the limit of a fine discretization, the same is not true for the radiative contribution calculated with Eq. (6). In Eq. (6) it is assumed that the plasmonic structure jointly to the emitter acts as a unique radiating nanoantenna but since the fields emitted by each dipole interfere with each other and with the fields directly emitted by the dipole, the phase difference between them should be considered for large objects or for big emitter–metal distances. In the next paragraphs we will refer to this method as the approximated one of Γ_R; we will see that Eq. (6) gives the exact values of the radiative decay rate for small enough nanoparticles for which phase retardations are

minimal (Fig. 2b), while it fails for larger nanoparticles (Fig. 5b).

3. Results and discussion

In this section the normalized absorption efficiencies as well as the total, radiative and nonradiative decay rates of Ag elongated nanoparticles, i.e. spheroid, cone and solid rhombus, will be presented. In particular, attention will be paid on the possibility to realize an electromagnetic coupling between plasmonic modes and far-field radiation. For normalization absorption efficiency we will intend the DDA absorption efficiency normalized to the squared modulus of the dipole (NAE $= Q_{\rm abs}/|\tilde{\mathbf{p}}_0|^2$), this being mandatory to obtain spectra independent of the source. The DDA efficiency $Q_{\rm abs}$ is calculated, as usual, by dividing the absorption cross section over the area of the geometrical cross section of the sphere with volume equal to that of the dipole representation of the particle ($\pi a_{\rm eff}^2$). Unless otherwise specified, the Palik dielectric function [45] and an interdipole distance of $d_{\rm int} = 0.0625 = 1/16$ nm are used in describing the metallic nanostructures. For spherically shaped nanoparticles the adopted prescription for the discretization parameter $d_{\rm int}$=1/16 nm, has been proved to be good enough by recurring to a comparison with the analytical results [25,26]. In [26] it has been shown that for nanospheres, which are more difficult to be treated than cubically shaped nanoparticles, a discretization parameter $d_{\rm int} = 1/16$ nm yields results with an accuracy better than 5% for the total and nonradiative decay rates and of the order of 10% for the radiative one, and this in agreement with the idea expressed in the work of Yurkin et al. [35] that DDA errors are larger for the absorption with respect to scattering. In the same work [26], convergence tests have also been reported for exactly the same sharp-tip nanocone here analyzed excited by a dipole located at 2 nm from the tip.

3.1. High-order modes vs far field radiation: the spheroid case

Differently from the case of an equivalent diameter sphere, if we excite Ag prolate spheroids with a near dipole oscillating along the symmetry axis, due to shape anisotropy we can observe the appearance of multiple resonances. In Fig. 1a the normalized absorption efficiencies are reported for two Ag prolate spheroids with a 20 nm major axis and two different aspect ratios (2 and 4) excited with a 2 nm far dipole aligned to the symmetry axis (z).

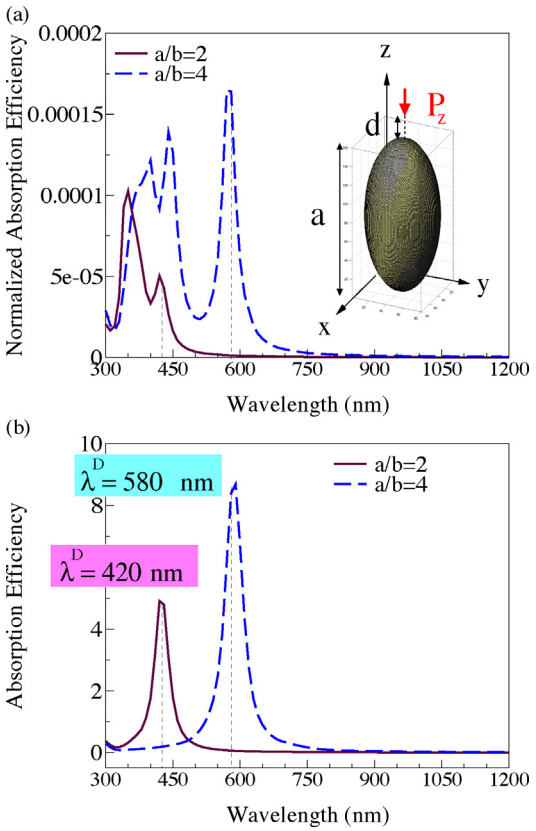

Fig. 1. (a) Normalized absorption efficiencies for two Ag prolated spheroids with a 20 nm major axis (a) and aspect ratios (a/b) 2 and 4 excited by a dipole oscillating along the symmetry axis (z) at 2 nm from the surface. (b) Absorption efficiencies for the same particles in (a) excited with a plane wave polarized along z. The marked resonances in (b) are the dipole resonances corresponding to the peaks at smaller energies in the spectra in panel (a).

As it can be observed if compared to the ones obtained for a plane wave polarized along z (Fig. 1b), these spectra present several peaks corresponding to plasmonic resonances of several orders. The same rich structure can be recognized also in the decay rate spectra in Fig. 2a.

The total decay rates, for these small nanoparticles, seem in fact to be almost completely due to the losses inside metal and to perfectly trace the nonradiative decay rates calculated with Eq. (3). For what concerns the radiative decay rates, the only contributions to the decay can be ascribed to the dipole radiation. Γ_R calculated by difference between the total and the nonradiative ones, matches exactly the radiative decay rate calculated for the two nanoparticles according to Eq. (6) (Fig. 2b). A second peak is observed in both the nonradiative decay rate spectra at larger energies with respect to the dipolar one, but this is absent in the

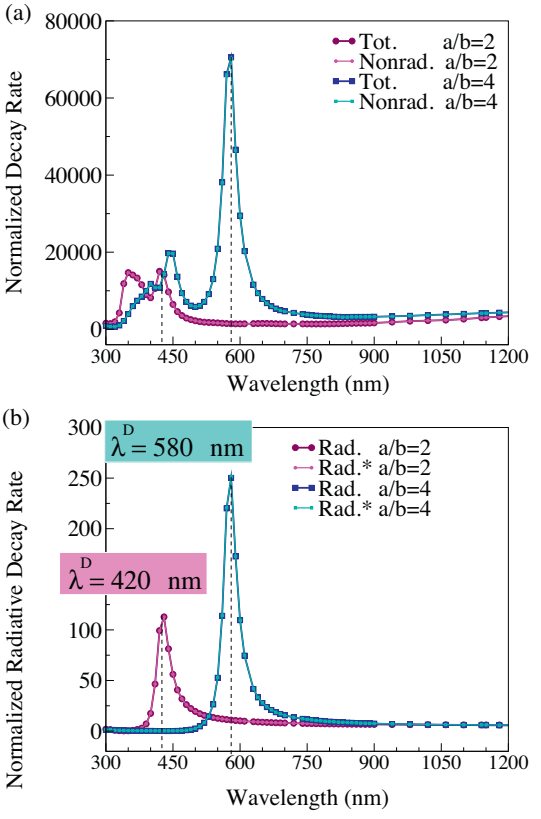

Fig. 2. (a) Normalized total and nonradiative decay rates for two Ag prolated spheroids with a 20 nm major axis (a) and aspect ratios (a/b) 2 and 4 excited by a dipole oscillating along the symmetry axis (z) at 2 nm from the surface. (b) Radiative decay rates for the particles in (a) calculated with the approximation in Eq. (6) and indirectly or by difference $\Gamma_R = \Gamma - \Gamma_{NR}$ (*). (For interpretation of the references to color in this figure legend, the reader is referred to the web version of the article.)

radiative decay (Fig. 2b) and in the far-field absorption (Fig. 1b) [46].

The physical nature of the two resonances appearing in Γ_R at $\lambda_{exc} = 420$ nm and $\lambda_{exc} = 580$ nm for the two different aspect ratios (Fig. 2a) can be clarified by observing the charge distributions in Figs. 3 and 4, respectively.

To have an intuitive picture of the induced electronic charge, in Figs. 3 and 4, $\rho(\mathbf{r})$ is transformed into a one-variable function $Q(x)$ by integrating its real part on slices with a thickness $d = 1$ nm perpendicular to the chosen direction

$$Q(x, \lambda_{exc}) = \int_{x-d/2}^{x+d/2} \int\int \rho_i(x', y', z', \lambda_{exc})\, dx'\, dy'\, dz'. \tag{7}$$

Resonances at $\lambda_{exc} = 420$ nm for $a/b = 2$ (Fig. 3c and d) and at $\lambda_{exc} = 580$ nm (Fig. 4e and f) correspond to the

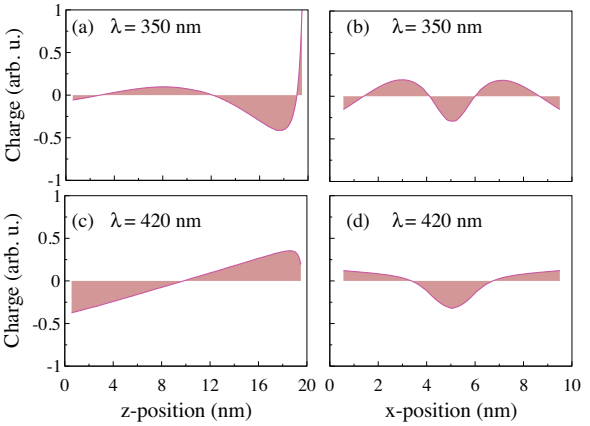

Fig. 3. Charge distributions along the symmetry direction (z) and the minor axis direction (x) obtained for the two resonances in the spectrum of the spheroid with $a = 20$ nm and $a/b = 2$ (violet line in Fig. 2a): $\lambda_{exc} = 350$ nm (a and b) and $\lambda_{exc} = 420$ nm (c and d).

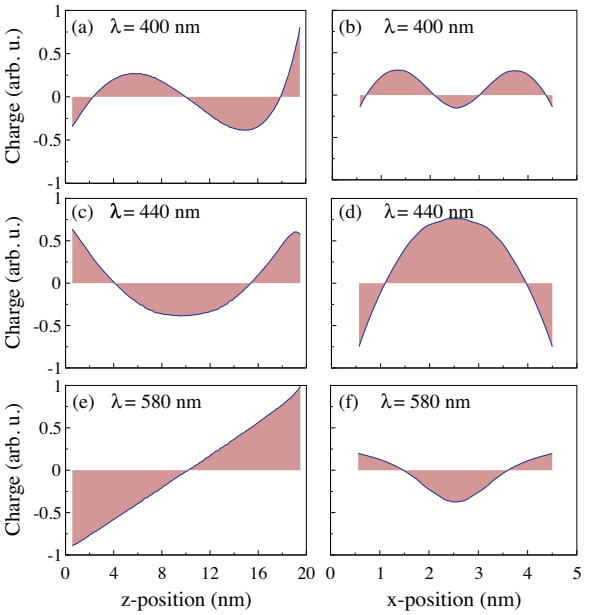

Fig. 4. Charge distributions along the symmetry direction (z) and the minor axis direction (x) obtained for the three resonances in the spectrum of the spheroid with $a = 20$ nm and $a/b = 4$ (blue line in Fig. 2a): $\lambda_{exc} = 400$ nm (a and b), $\lambda_{exc} = 440$ nm (c and d) and $\lambda_{exc} = 580$ nm (e and f).

same mode: with a clear dislocation of charge density along the symmetry and the appearance of two opposite sign regions along z, they are both dipolar modes. The higher energy resonances present a number of nodes in the charge distribution: one node corresponds to a dipole, two nodes corresponds to a quadrupole, etc. The higher-order modes present charge densities

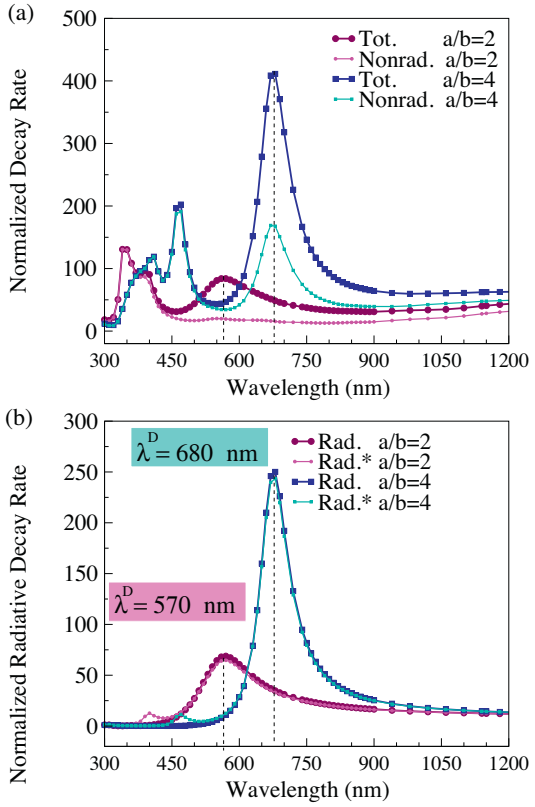

Fig. 5. (a) Normalized total and nonradiative decay rates for two Ag prolated spheroids with a 160 nm major axis (a) and aspect ratios (a/b) 2 and 4 excited by a dipole oscillating along the symmetry axis (z) at 10 nm from the surface. (b) Radiative decay rates for the particles in (a) calculated with the approximation in Eq. (6) and indirectly or by difference $\Gamma_R = \Gamma - \Gamma_{NR}$ (*). (For interpretation of the references to color in this figure legend, the reader is referred to the web version of the article.)

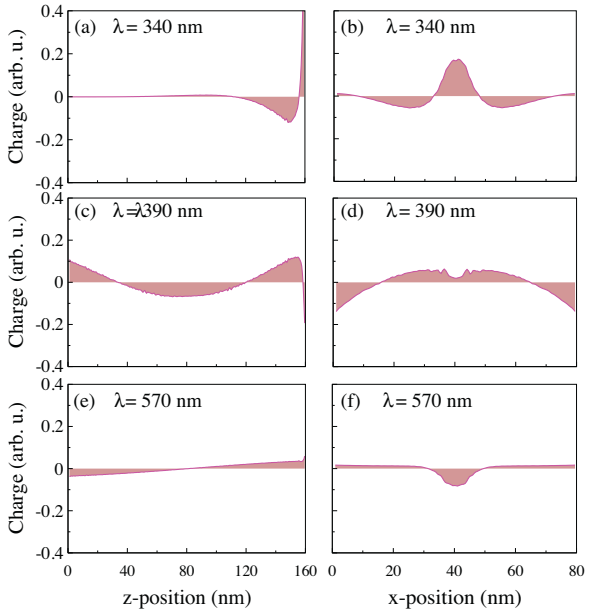

Fig. 6. Charge distributions along the symmetry direction (z) and the minor axis direction (x) obtained for the three resonances in the spectrum of the spheroid with $a = 160$ nm and $a/b = 2$ (violet line in Fig. 5a): $\lambda_{exc} = 340$ nm (a and b), $\lambda_{exc} = 390$ nm (c and d) and $\lambda_{exc} = 570$ nm (e and f).

comparable with the dipolar ones but a zero net dipole moment. Thus, even though the field enhancement near the surface is as large as for the dipolar mode, the radiative enhancement is absent for these modes and they appear dark. Anyway, if higher-order modes are completely radiationless in the quasistatic approximation, due to phase retardations they can acquire a non null net dipole moment inside large nanoparticles. To verify this phenomenon we thus move from small spheroids to larger ones. As it can be seen in Fig. 5a, by enlarging the major axis of the prolate spheroid from 20 nm to 160 nm higher-energy peaks become more evident and distinguishable, with the third resonance appearing also for an aspect ratio of 2.

While the charge distributions for the three resonances obtained at 340 nm, 390 nm and 570 nm for a 160 nm spheroid with $a/b = 2$ (Fig. 6) are exactly the same of smaller spheroids, the balance between radiation and losses is completely different. For large spheroids in fact the major contribution to Γ at the dipole frequency is due to Γ_R and small peaks appear also for higher-order modes. By indirectly calculating Γ_R we have two features at 400 nm and 470 nm for a/b 2 and 4, respectively (Fig. 5b).

Due to phase retardation, quadrupolar modes, like those in Fig. 6b and c, assume thus the character of bright modes, contrary to common belief that even modes are dark and unable to couple to far-field radiation [46]. Their coupling to far-field radiation is surely weaker than the dipole one but it cannot be neglected. Eq. (6) well approximates the radiative decay rate at the dipole resonance, where the dipoles oscillate in phase and the plasmonic structure acts as a unique radiating nanoantenna, but it fails in describing the contribution at the higher-order resonances, where radiation from multipoles should be considered.

3.2. Far field radiation vs high-order modes: the cone case

The coupling of far-field radiation with high-order modes can also be found in the absorption spectrum of conically shaped nanoparticles. Until now we have just applied our method to cases which can be solved

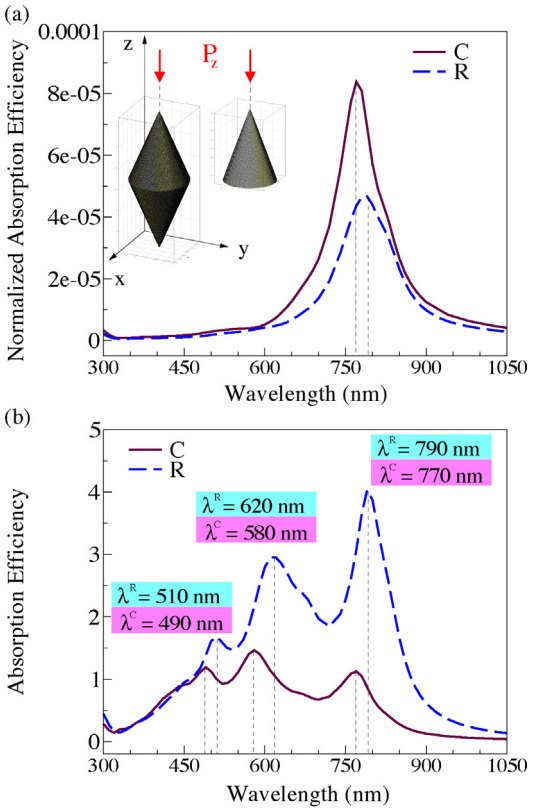

Fig. 7. Normalized absorption efficiencies for a 20 nm high Ag cone (C) and a 40 nm high solid rhombus (R) with bases of 10 nm diameter, excited by a dipole oscillating along the symmetry axis (z) at 2 nm from the surface. (b) Absorption efficiencies for the same particles in (a) excited with a plane wave polarized along z.

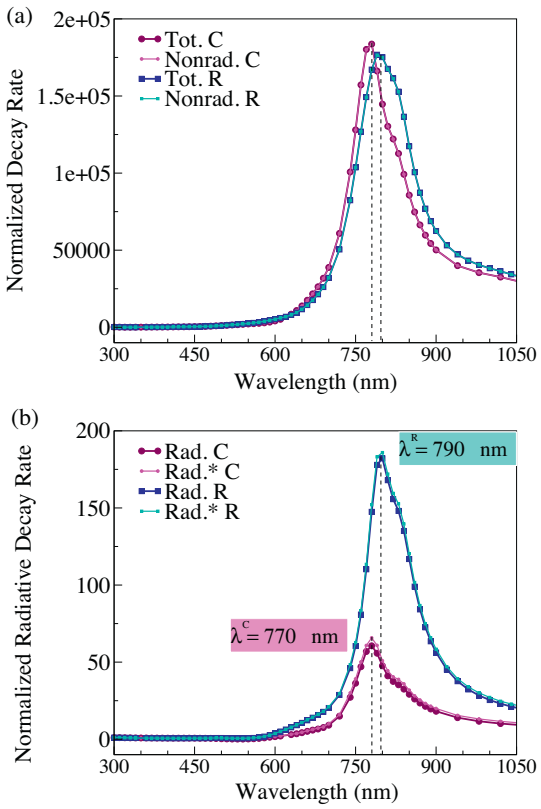

Fig. 8. (a) Normalized total and nonradiative decay rates for the cone (C) and the solid rhombus (R) in Fig. 7a. (b) Radiative decay rates for the particles in (a) calculated with the approximation in Eq. (6) and indirectly or by difference $\Gamma_R = \Gamma - \Gamma_{NR}$ (*).

analytically [47]. From here on we will focus on conically shaped nanoparticles acting as nanoantennas, and in particular we will analyze a 20 nm high Ag nanocone and a 40 nm high Ag solid rhombus with bases of 10 nm, both excited by a dipole oscillating along the symmetry axis at 2 nm from the tip (see the sketch in Fig. 7), as well as by a plane wave polarized along the symmetry axis.

Similarly to what observed for the prolate spheroids, we expect sharp nanocones to support a series of resonances associated with higher-order surface plasmon modes. The normalized absorption efficiency spectra obtained for the cone and the rhombus excited by a near-source radiation are reported in Fig. 7a and compared with the spectra calculated by considering a plane wave polarized along the z direction (Fig. 7b).

For the cone we can observe that, with a source at 2 nm from the tip, only the lower-energy mode can be excited at a wavelength of 770 nm (Fig. 7a). Otherwise, by radiating the same target with a plane wave, the spectrum becomes broader with two further peaks at 490 nm and 580 nm and a shoulder on the short-wavelength side. The spectrum for a dipolar excitation has been shown to gradually change at increasing distance from the tip and to become similar to the plane wave one already at 50 nm [26]. The same counter-intuitive behavior seems to appear also for the 40 nm rhombus excited at the same conditions with the three resonances red-shifted at 510 nm, 620 nm and 790 nm. The total, radiative and nonradiative decay rates obtained for the two structures excited with a dipole at 2 nm are reported in Fig. 8. Consistently with the absorption effieciency in Fig. 7a, only a peak at 770 nm for the cone and 790 nm for the rhombus are observed. If compared to the spheroid case, we can notice the huge enhancement of the decay rate induced by conically shaped nanoparticles (Fig. 8a): the lifetime of the dipole is reduced by 3 orders of magnitude by moving from a 20 nm spheroid to a 20 nm cone.

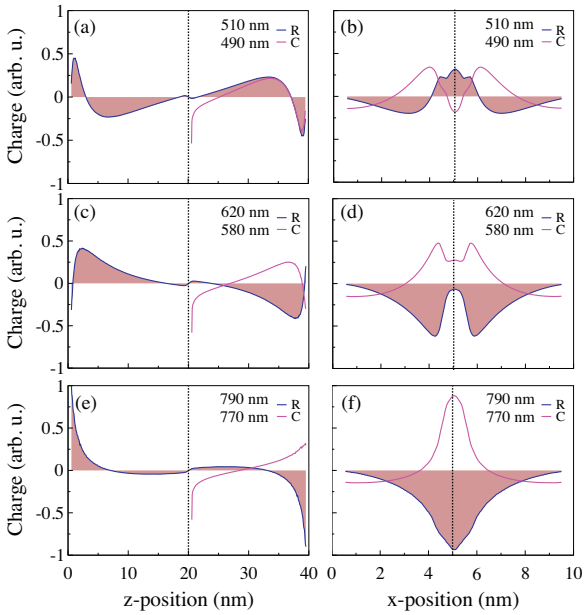

Fig. 9. Charge distributions along the symmetry direction (z) and the minor axis direction (x) obtained for the three resonances in the spectrum (Fig. 7b) of the solid rhombus (R): $\lambda_{exc} = 510$ nm (a and b), $\lambda_{exc} = 620$ nm (c and d) and $\lambda_{exc} = 790$ nm (e and f). Charge distributions reported in panels (b), (d) and (e) are obtained by making a summation of charge over half target in z direction, the summation all over the target giving null quantities. The pink curves plotted above the rhombus charge distributions (blue lines) report, for comparison, the charge distributions obtained for the cone (C) at the corresponding resonances: $\lambda_{exc} = 490$ nm (a and b), $\lambda_{exc} = 580$ nm (c and d) and $\lambda_{exc} = 770$ nm (e and f). (For interpretation of the references to color in this figure legend, the reader is referred to the web version of the article.)

The presence of several resonant peaks for far-field excitations can be reconduced to the tip shape and an explanation can be found in the charge distributions reported in Fig. 9. All the resonances involve charge oscillations localized in proximity of the tip and thus strongly related to the conical shape of both the structures.

As expected, the three resonances in the spectra of the two structures in Fig. 7b correspond to the same plasmonic modes, the red-shift being due to the charge density perturbation at the central region of the rhombus. As it can be observed from the charge dislocation along the height of the rhombus, the resonance at 790 nm looks like a dipole mode with an important net dipole moment (Fig. 9e): this can therefore be excited by both radiation sources here considered. The resonances appearing at higher energies (620 nm and 510 nm) instead, seem to be related to higher order-modes, being the number of nodes in the charge distribution larger that one (Fig. 9). In both these resonances the two asymmetrically distributed regions of induced charge radiate as antiparallel dipoles but, differently from what happens for structures symmetric along the radiation polarization, they do not yield a vanishing net dipole along z, this being responsible for the electromagnetic coupling of even modes (dark in a symmetric structure) with a plane wave radiation. While from symmetry considerations the dipole could couple with all the resonances excited by the plane wave, the behavior of the field lines evolves with the distance between the dipole source and the tip, causing the appearance of resonances at increasing metal-dipole distance. The results of Fig. 7 therefore show that small conically-shaped nanoparticles can support several plasmonic resonances in the VIS spectral range also for far-field excitations. Moreover the spectrum as a function of radiation and metal–emitter separation [26], can be exploited to get information on the metal–emitter distance in actual experiments.

4. Conclusions

An useful numerical approach based on the Discrete Dipole Approximation is here applied to investigate the behavior of metallic antennas. The possibility to numerically calculate the total, radiative and nonradiative decay rate perturbations induced by a nanoparticle on the dynamics of a punctual emitter as well as the absorption spectrum can be very promising in molecular plasmonics. In particular the focus is put on the capability of high-order modes to couple to far-field radiation. An analysis performed on large Ag prolate spheroids has underlined the error done in neglecting the radiation contributions beyond the dipolar one. Calculations done on conically shaped nanoparticles have instead presented a counterintuitive behavior of this kind on nanoparticles: by moving from a far-field radiation to a dipolar one we have the disappearance of the high order resonances and this is contrary to the behavior of spheroids and other particles. We believe that these results demonstrate the importance of a numerical engineering of the dipole decay dynamics exploiting localized surface plasmons, in view of an aware experimental manipulation and tuning of decay processes in fluorescence spectroscopy applications.

Acknowledgments

This work was funded by Fondazione Cariplo under project no. 2010-0523 and by the European Research

Council (ERC) Starting Grant Project DEDOM, Grant Agreement No. 207441.

References

[1] S. Khn, U. Hakanson, L. Rogobete, V. Sandoghdar, Enhancement of single-molecule fluorescence using a gold nanoparticle as an optical nanoantenna, Physical Review Letters 97 (2006) 017402–17411.

[2] J.A. Schuller, E.S. Barnard, W.S. Cai, Y.C. Yun, J.S. White, M.L. Brongersma, Plasmonics for extreme light concentration and manipulation, Nature Materials 9 (2010) 193.

[3] P. Anger, P. Bharadwaj, L. Novotny, Enhancement and quenching of single-molecule fluorescence, Physical Review Letters 96 (2006) 113002–113011.

[4] O.L. Muskens, V. Giannini, J.A. Snchez Gil, J. Gmez Rivas, Strong enhancement of the radiative decay rate of emitters by single plasmonic nanoantennas, Nano Letters 7 (2007) 2871.

[5] H. Mertens, A.F. Koenderink, A. Polman, Plasmon-enhanced luminescence near noble-metal nanospheres: comparison of exact theory and an improved Gersten and Nitzan model, Physical Review B 76 (2007) 115123–115131.

[6] G.W. Ford, W.H. Weber, Electromagnetic interactions of molecules with metal surfaces, Physics Reports 113 (1984) 195.

[7] A. Moroz, Superconvergent representation of the Gersten–Nitzan and Ford–Weber nonradiative rates, Journal of Physical Chemistry C 115 (40) (2011) 19546.

[8] H. Metiu, Surface enhanced spectroscopy, Progress in Surface Science 17 (1984) 153.

[9] L. Novotny, B. Hecht, Principles of Nano-Optics, Cambridge University Press, New York, 2006.

[10] S. Kuhn, G. Mori, M. Agio, V. Sandoghdar, Modification of single molecule fluorescence close to a nanostructure: radiation pattern, spontaneous emission and quenching, Molecular Physics 106 (2008) 893.

[11] M. Moskovits, Surface-enhanced spectroscopy, Reviews of Modern Physics 57 (1985) 783.

[12] E. Castani, M. Boffety, R. Carminati, Fluorescence quenching by a metal nanoparticle in the extreme near-field regime, Optics Letters 35 (2010) 291.

[13] J.E. Sipe, New Green-function formalism for surface optics, Journal of the Optical Society of America B 4 (1987) 481.

[14] C. Vandenbem, D. Brayer, L.S. Froufe-Prez, R. Carminati, Controlling the quantum yield of a dipole emitter with coupled plasmonic modes, Physical Review B 81 (2010) 085444–85451.

[15] C. Vandenbem, L.S. Froufe-Perez, R. Carminati, Fluorescence signal of a single emitter coupled to a nanoparticle through a plasmonic film, Journal of Optics A: Pure and Applied Optics 11 (2009) 114007–114011.

[16] L. Novotny, Single molecule fluorescence in inhomogeneous environments, Applied Physics Letters 69 (1996) 3806.

[17] R. Carminati, J.-J. Greffet, C. Henkel, J.M. Vigoureux, Radiative and non-radiative decay of a single molecule close to a metallic nanoparticle, Optics Communications 261 (2006) 368.

[18] V. Giannini, J.A. Snchez-Gil, O.L. Muskens, J. Gmez Rivas, Electrodynamic calculations of spontaneous emission coupled to metal nanostructures of arbitrary shape: nanoantenna-enhanced fluorescence, Journal of the Optical Society of America B 26 (2009) 1569.

[19] L.S. Froufe-Prez, R. Carminati, Lifetime fluctuations of a single emitter in a disordered nanoscopic system: the influence of the transition dipole orientation, Physica Status Solidi (a) 205 (2008) 1258.

[20] L.S. Froufe-Prez, R. Carminati, Fluorescence decay rate statistics of a single molecule in a disordered cluster of nanoparticles, Physical Review A 76 (2007) 013835–13841.

[21] J.W. Liaw, J.H. Chen, C.S. Chen, M.K. Kuo, Purcell effect of nanoshell dimer on single molecule's fluorescence, Optics Express 17 (2009) 13532.

[22] M. Thomas, J.J. Greffet, R. Carminati, J.R. Arias Gonzalez, Single-molecule spontaneous emission close to absorbing nanostructures, Applied Physics Letters 85 (2004) 3863.

[23] A. Mohammadi, F. Kaminski, V. Sandoghdar, M. Agio, Fluorescence enhancement with the optical (bi-)conical antenna, Journal of Physical Chemistry C 114 (2010) 7372.

[24] S. D'Agostino, F. Della Sala, L.C. Andreani, Dipole decay rates engineering via silver nanocones, Plasmonics (2013), http://dx.doi.org/10.1007/s11468-013-9512-3, Published online: 01 March 2013.

[25] S. D'Agostino, F. Della Sala, L.C. Andreani, Dipole decay rates engineering via metallic nanosystems, AIP Conference Proceedings 1475 (2012) 47.

[26] S. D'Agostino, F. Della Sala, L.C. Andreani, Dipole-excited surface plasmons in metallic nanoparticles: engineering decay dynamics within the discrete-dipole approximation, Physical Review B 87 (2013) 205413.

[27] A.B. Evlyukhin, C. Reinhardt, B.N. Chichkov, Multipole light scattering by nonspherical nanoparticles in the Discrete Dipole Approximation, Physical Review B 84 (2011) 235429.

[28] R.R. Alfano, Advances in ultrafast time resolved fluorescence physics for cancer detection in optical biopsy, AIP Advances 2 (2012) 011103.

[29] M.R. Gartia, A. Hsiao, M. Sivaguru, Y. Chen, G.L. Liu, Enhanced 3D fluorescence live cell imaging on nanoplasmonic substrate, Nanotechnology 22 (2011) 365203.

[30] L. Novotny, E.J. Sanchez, X.S. Xie, Near-field optical imaging using metal tips illuminated by higher-order Hermite–Gaussian beams, Ultramicroscopy 71 (1998) 21.

[31] M. Ashino, M. Ohtsu, Fabrication and evaluation of a localized plasmon resonance probe for near-field optical microscopy/spectroscopy, Applied Physics Letters 72 (1998) 1299.

[32] B.T. Draine, P.J. Flatau, Discrete-dipole approximation for scattering calculations, Journal of the Optical Society of America A 11 (1994) 1491.

[33] M.A. Yurkin, A.G. Hoekstra, The discrete-dipole-approximation code ADDA: capabilities and known limitations, Journal of Quantitative Spectroscopy and Radiative Transfer 112 (2011) 2234.

[34] M.A. Yurkin, A.G. Hoekstra, ADDA, 2013 available at http://code.google.com/p/adda/.

[35] M.A. Yurkin, D. de Kanter, A.G. Hoekstra, Accuracy of the Discrete Dipole Approximation for simulation of optical properties of gold nanoparticles, Journal of Nanophotonics 4 (2010) 041585.

[36] S. D'Agostino, P.P. Pompa, R. Chiuri, R.J. Phaneuf, D.G. Britti, R. Rinaldi, R. Cingolani, F. Della Sala, Enhanced fluorescence by metal nanospheres on metal substrates, Optics Letters 34 (2009) 2381.

[37] K.J. Vahala, Optical microcavities, Nature 424 (2003) 839.

[38] P. Goy, J.M. Raimond, M.M. Cross, S. Haroche, Observation of cavity-enhanced single-atom spontaneous emission, Physical Review Letters 50 (1983) 1903.

[39] G. Gabrielse, H. Dehmelt, Observation of inhibited spontaneous emission, Physical Review Letters 55 (1985) 67.

[40] M. Bayer, T.L. Reinecke, F. Weidner, A. Larionov, A. McDonald, A. Forchel, Inhibition and enhancement of the spontaneous emission of quantum dots in structured microresonators, Physical Review Letters 86 (2001) 3168.
[41] E.M. Purcell, Spontaneous emission probabilities at radio frequencies, Physical Review 69 (1946) 681.
[42] J. Gersten, Topics in Fluorescence Spectroscopy, vol.8: Radiative Decay Engineering, Springer Science + Business Media, New York, 2005.
[43] J. Gersten, A. Nitzan, Spectroscopic properties of molecules interacting with small dielectric particles, Journal of Chemical Physics 75 (1981) 1139.
[44] J.D. Jackson, Classical Electrodynamics, 3rd ed., John Wiley & Sons, Berkeley, 1999.
[45] E.D. Palik, Handbook of Optical Constants of Solids, Academic Press, New York, 1985.
[46] M. Liu, T.W. Lee, S.K. Gray, P. Guyot Sionnest, M. Pelton, Excitation of dark plasmons in metal nanoparticles by a localized emitter, Physical Review Letters 102 (2009) 107401.
[47] H. Mertens, A. Polman, Strong luminescence quantum efficiency enhancement near prolate metal nanoparticles: dipolar versus higher-order modes, Other Condensed Matter (2007), arXiv:0711.1591 [cond-mat.other].